Supporting Information

Molecular simulation studies on the design of energetic ammonium dinitramide co-crystals for tuning hygroscopicity

Zhongqi Ren[a], Xinjian Chen[a], Guojia Yu[a], Yinglei Wang[b], Bin Chen*[b], and Zhiyong Zhou*[a]

[a]College of Chemical Engineering, Beijing University of Chemical Technology, Beijing 100029, People's Republic of China

[b]Xi'an Modern Chemistry Research Institute, 168 Zhangba Rd. East, Xi'an 710065, People's Republic of China

*Corresponding author: zhouzy@mail.buct.edu.cn (Zhiyong Zhou); cb204s@163.com (Bin Chen)

Contents

2.2 Predictive packing diagrams of co-crystals

2.3 The lowest energy water sorption frames of co-crystal surfaces

3. Table captions

4. Calculations related to ADN/18C6 co-crystal

5. Predicted ADN/CL-20, ADN/HMX, ADN/18C6 co-crystal morphology by BFDH method and water total sorption capacity

Table S11. The computational water sorption capacity of ADN/CL-20, ADN/HMX, ADN/18C6 co-crystal surface

6. References

1. Computational method and details

1.1 Initial selection and the molecular structures of energetic materials

Selection of energetic materials co-former needs multi-aspect consideration. High performance and low sensitivity usually are a standard of assessing energetic materials. Because of lack of research on hygroscopicity of energetic materials, some common explosives were selected as the co-formers, due to their relatively mature preparation technologies.

Nine energetic materials (EMS) containing CL-20, BTF, HMX, TNT, ETN, RDX, TNB, MATNB and TNAZ were selected as co-crystal co-formers. Fig. 1 shows molecular structures of nine selected energetic materials, which can be classified as different types according to molecular structures. The selected molecular structure types include linear structure, cyclic structure and cage-like structure. A series of their properties including density, detonation velocity (V_d), detonation pressure (P_d), oxygen balance (OB), oxygen balance after 1:1 co-crystallization (OBAC) and gas formed by 1 g energetic materials at pressure of 1 bar (V_{gas}) are listed in Table S1.[1-4] The OB and OBAC values can be calculated by Eq.1.

$$OB = \frac{\left[c - \left(2a + b/2\right)\right]}{M_{\mathrm{r}}} \times 16 \times 100\% \qquad (1)$$

where *a*, *b* and *c* are the numbers of C, H and O atoms in one molecule, respectively, M_r represents the relative molecular mass. The details of calculating oxygen balance after forming 1:1 co-crystallization are shown in Table S2 in the Supporting Information.

Some energetic materials like RDX and HMX have been used as components of propellants.[5,6] Compared with these energetic materials, it is easy to find that ADN as a propellant component has advantages of higher OB and V_{gas}. However, how to improve ADN hygroscopicity and estimate water sorption capacity of energetic co-crystal materials are the highlights in this work.

1.2 Molecular electrostatic potential calculations of ADN and co-crystal guests.

The molecular electrostatic potential surfaces (MEPS) of the component molecules of interest are usually employed to understand the molecular packing in their co-crystals.[7-9] In the rules of crystal packing, the place with positive electrostatic potential of one molecule combines with the place at where there is negative electrostatic potential of the other molecule. The electrostatic potential (V(r)) that the nuclei and electron in a molecule create at any point r in the surrounding space is given by Eq. 2.[10]

$$V\left(r\right) = \sum_{\mathrm{A}} \frac{Z_{\mathrm{A}}}{\left|R_{\mathrm{A}} - r\right|} - \int \frac{\rho\left(r'\right)dr'}{\left|r' - r\right|} \qquad (2)$$

where Z_A is the charge on nucleus A, which is located at R_A, ρ(r) is the electronic density of molecule. The surface which reflects the specific features of each molecule can be defined as the ρ(r) contours.[10]

By calculating the MEPS, intermolecular H-bonding sites and N-H…O supramolecular synthon can be found in ADN co-crystals. The functional GGA-BLYP and the basis set DNP-3.5 were used for geometry optimization in Dmol3 module. The selected properties were electron density and electrostatics. At last, transparency of electrostatic potential was adjusted to make

the presentation clearer.

1.3 Prediction of possible co-crystal lattice structure

The properties of a material depend very sensitively on its structure.[11] The properties of crystal materials depend on not only molecular structure but also co-crystal lattice structure. The prediction calculations of co-crystals' structures were based on Monte Carlo method.

First, intermolecular structure optimization needs multiple tentative calculations, in which relative position also changes. After multiple optimizations of co-crystal intermolecular structure, minimum lattice energy can be obtained. In this section, the mode of co-crystal interaction is mainly between NH_4^+ of ADN and oxygen atoms of co-crystal guest, according to previous calculation results of molecular electrostatic potential.

Then, the polymorph predictive method was used to simulate co-crystal lattice structures and a large amount of crystal structures were obtained. The lattice energy and co-crystal density values were calculated by placing the relative positions of molecules in the crystal cell continuously. This method can well predict the crystal space group, and obtain the predictive crystal cell parameters, H-bonding energy, lattice energy and co-crystal density.

Since the Dreiding force field, as a generic force field, can well describe interaction between ADN and other energetic molecules,[12,13] the Dreiding force field was used in the molecular structures and crystal structures optimization processes. Medium quality, clustering option and atom-based summation method was selected. Explore torsion degree of freedom and the Pre-optimization were set to get accurate structures. Ten space groups including P-21/C, P-1, P212121, C2/C, P21, PBCA, PNA21, CC, PBCN and C2 were selected. The H-bond energy term in the Dreiding force field is given by Eq. 3.

$$E_{\mathrm{hb}} = D_{hb}\left[5\left(R_{hb}/R_{DA}\right)^{12} - 6\left(R_{hb}/R_{DA}\right)^{10}\right]\cos^4\left(\theta_{DHA}\right) \qquad (3)$$

Where θ_{DHA} is the bond angle between the hydrogen donor (D), the hydrogen (H), and the hydrogen acceptor (A), where R_{DA} is the distance between the donor and acceptor atoms. The values of D_{hb} and R_{hb} depend on the convention for assigning charges.

Most researchers are inclined to think that the lowest crystal lattice energy is the rule of selecting crystal structure, and the crystals with the lowest lattice energy are thermodynamically most stable compared with crystals of other structures.[14] In some cases, the maximum density of crystal structure is equal to the lowest energy of crystal structure.[15] What needs to be emphasized is that the selected structure by crystal structure prediction may be inaccurate compared with the experimental values. The experimental structure is hidden generally amongst the 100 or so lowest-energy structures.[16,17] However, it is convenience to build and select one co-crystal structure from more than two thousand structures for one kind of co-crystals.

1.4 Water sorption capacity on co-crystal surface

In our previous work,[18] water sorption capacity of ADN crystal has been studied, and the computational results were in good agreement with the experimental ones. The calculation parameters as well as the calculation method of this section are as same as those reported in our previous work. Water sorption capacity calculations have its origins in "adsorbed phase" defined by Gibbs.[19] Gibbs defined the "adsorbed phase" as the actual amount of gas minus the amount of gas which would be presented in the same space at the prevailing bulk density of the gas to avoid the question: how close to the surface must a molecule be in order to be classified as adsorbed. Saturated adsorption capacity was calculated by Eq.4

$$n_{ex} = n_{ab} - \rho_g V_a \qquad (4)$$

where n_{ex} is the saturated adsorption capacity, n_{ab} is called as the absolute adsorption capacity, ρ_g is the density of the equilibrium gas phase, and V_a is the volume of adsorbed phase.

The 2 × 2 × 2 ADN or co-crystals supercell was cleaved with 1.0 factional thickness to create

the required surfaces. The (100), (010) and (001) crystal faces, which are called basic crystal faces, are common and simple crystal surfaces. Basic crystal faces are with low indices of crystal face and important parts of crystal surfaces. To avoid the additional free boundary effect, a 10 Å vacuum slab and repetitive unit were added by constructing 1 × 1 × 2 supercell. At last, excessive vacuum slabs were removed by adjusting crystal lattice parameters. The middle part of the model is vacuum slab on behalf of the region of wet air, which is shown in Figure S10-S18 in the Supporting Information. The water sorption capacity of ADN increases with the increase of temperature and propellants are sometimes used under harsh conditions. Therefore, the condition was set as 308.15 K and 50% relative humidity to compare performance of resisting water sorption. The ensemble was μVT, in which the chemical potential μ, volume V, and temperature T are constant in the simulation process. The Dreiding force field with the Gasteiger charges, Ewald and atom-based summation methods for electrostatic and van der Waals interactions, respectively, were employed to calculate water sorption heat.

Since the hygroscopicity of crystal is dominated by the crystal surface, the hygroscopicity of co-crystal must be different from pure crystal. Comparing water sorption capacity and water sorption heat of different co-crystals, the hygroscopicity of different co-crystals can be estimated.[18,20] The model and calculation parameters can be used to predict other ADN-based energetic co-crystal materials. It is convenient and quick to predict crystal hygroscopicity without experiment, which can speed up the research and development of new energetic co-crystal materials for tuning physical properties.

1.5 The interaction between water molecule and crystal surface

The interaction between water molecule and crystal surface can be investigated by molecular mechanics simulations.[21] Based on computational results of water sorption capacity, the co-crystals with low water sorption capacity such as CL-20/ADN, HMX/ADN,18C6/ADN are used to investigate the interaction between water molecule and crystal surface and verify the reliability of water sorption capacity calculations. The calculation method is as follow. Create 2×2×2 supercell, cleave (1 0 0), (0 1 0) and (0 0 1) crystal surface, and add a vacuum layer of 30 Angstroms, add one water molecule in the vacuum layer, constrain the crystal plane. Forcite optimization is used to optimize the structure of the model. use Dreiding force field and Gasteiger calculation method. For the electrostatic force, the Ewald statistical accuracy is 0.00001 kcal/mol and 0.5 Angstrom is as the edge width. For the van der Waals force, a statistical method based on atoms is used, the truncation radius is set as 18.5 Angstroms, the total energy convergence is set to $1.0e^{-4}$ kcal/mol, and the force convergence is set to 0.005 kcal/mol/A. Due to the uneven surface of the crystal, the E_{int} may have different forces in different surface location. Therefore, the place on adding water molecule is set randomly in three time. Then take the average of E_{int}. The energy formula of the surface of the material and the water molecules is given by Eq. 5.

$$E_{\text{int}} = E_{surf+water} - E_{surf} - E_{water} \quad (5)$$

The E_{int}, $E_{surf+water}$, E_{surf} and E_{water} refer to the interaction between water molecule and crystal surface, the energy of crystal surface, the energy of crystal surface, the energy of water molecule respectively.

1.6 Virtual co-crystal screening calculations

Although many possible co-formers may have a good effect on reducing the water sorption capacity of ADN crystal, an important question has been proposed: “Whether all possible co-crystals can be formed experimental successfully?”. Virtual co-crystal screening as a prediction tool is used to understand co-crystal formation and molecular interaction, which has been experimentally verified. [22,23] The virtual co-crystal which assume some rules of co-crystal formation is a promising tool for focusing experimental efforts on the most promising crystal formers candidates. Firstly, Etters’ rule assumes two most polar interaction sites can be paired very likely. [24,25] Secondly, the energy between co-formers of co-crystal determines probability of

co-crystal formation. Thirdly, without attention for details of crystal packing, the potential interaction sites of two-dimensional structures are major consideration.

Based on molecular electrostatic potential surfaces of two-dimensional structures which is used to identify a discrete set of surface site interaction points, the value of the interaction site pairing energy difference △E as an important sign gives a good prediction result. Large surveys of co-crystals demonstrate that the co-crystals which can be formed must be more stable than the pure crystals. The high △E leads to the strong interactions between the two different components and formation of co-crystals is a high probability event.

$$E = -\sum_{ij} \alpha_i \beta_j \quad (6)$$

Where E is the interaction site pairing energy, and α_i are the H-bond donor parameters, and β_j are the H-bond acceptor parameters, and the sum represents the sum over all appropriately paired interaction sites.

$$\alpha = 0.0000162 MEP_{max}{}^2 + 0.00962 MEP_{max} \quad (7)$$

$$\beta = 0.000146 MEP_{min}{}^2 - 0.00930 MEP_{min} \quad (8)$$

where MEP_{min} and MEP_{max} are local minima and maxima on the MEPS in kJ/mol.

$$\Delta E = E_{cc} - nE_1 - mE_2 \quad (9)$$

where E_1 is the interaction site pairing energy of the pure form of component 1, E_2 is the interaction site pairing energy of the pure form of component 2, E_{cc} is the interaction site pairing energy of the co-crystal of stoichiometry 1n2m .As our research assumed, ADN and formers can be formed as the stoichiometry 1:1. Therefore, the parameters n, m in Eq.9 are set as 1.

$$P = \frac{e^{-(\Delta E + 11)/(RT)}}{1 + e^{-(\Delta E + 11)/(RT)}} \quad (10)$$

The Eq.10 is fitted from the caffeine and carbamazepine co-crystal data. When the -△E of co-crystals are more than 11kJ/mol, it is 50% probability that the co-crystals can be formed.[22] When △E are less than 0 kJ/mol, the co-crystals are inaccessible formed from the view of stability and thermodynamics. The larger -△E is, the more likely possibility of co-crystal formation is. Owe to uncertain experimental formation stoichiometry, the positive-negative judgment is used to evaluate the possibility of co-crystals and the P value is not given in the text.

2. Figure captions

2.1 Scatter diagrams of lattice energy and density of co-crystal

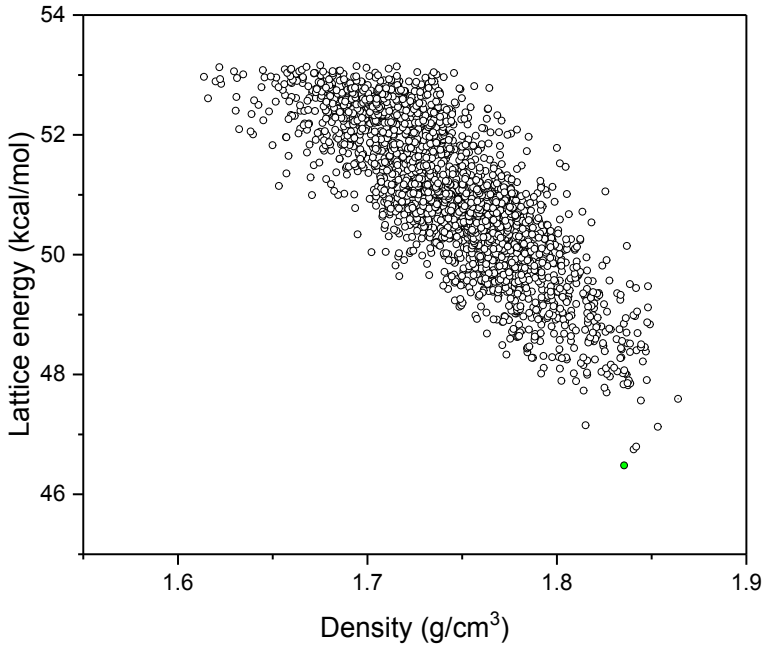

Figure S1. Scatter diagrams of lattice energy and density of co-crystal of ADN/CL-20

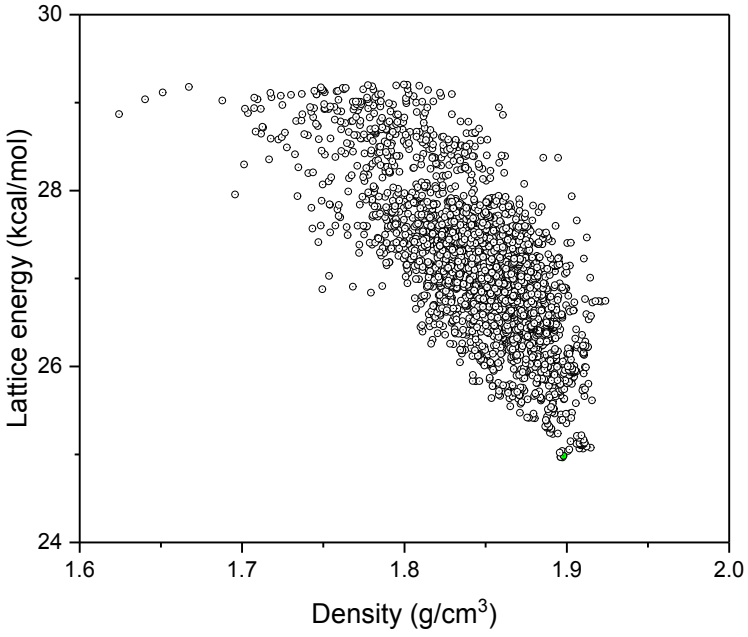

Figure S2. Scatter diagrams of lattice energy and density of co-crystal of ADN/BTF

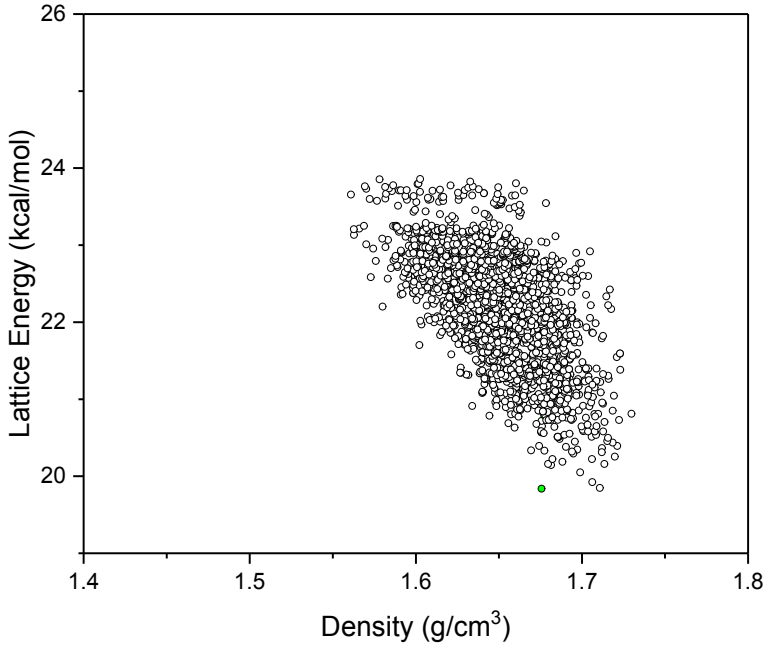

Figure S3. Scatter diagrams of lattice energy and density of co-crystal of ADN/HMX

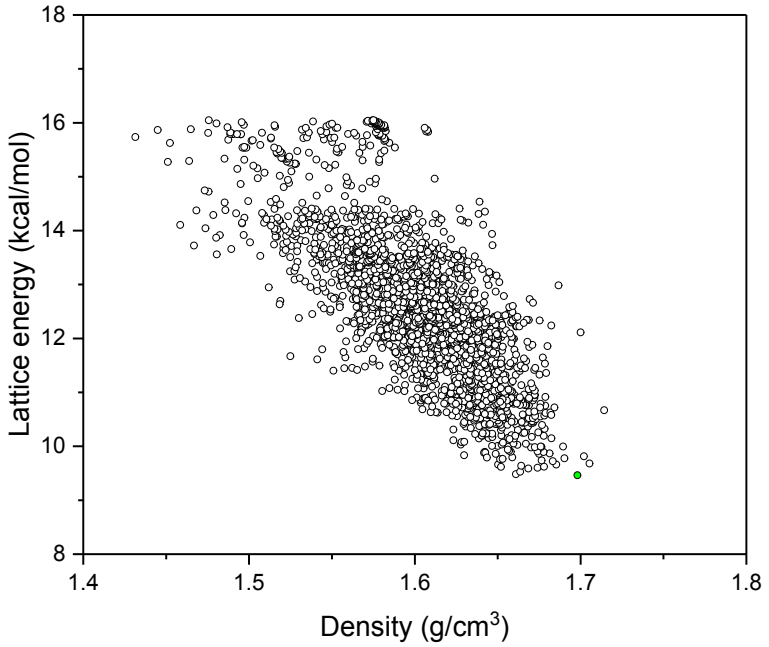

Figure S4. Scatter diagrams of lattice energy and density of co-crystal of ADN/TNT

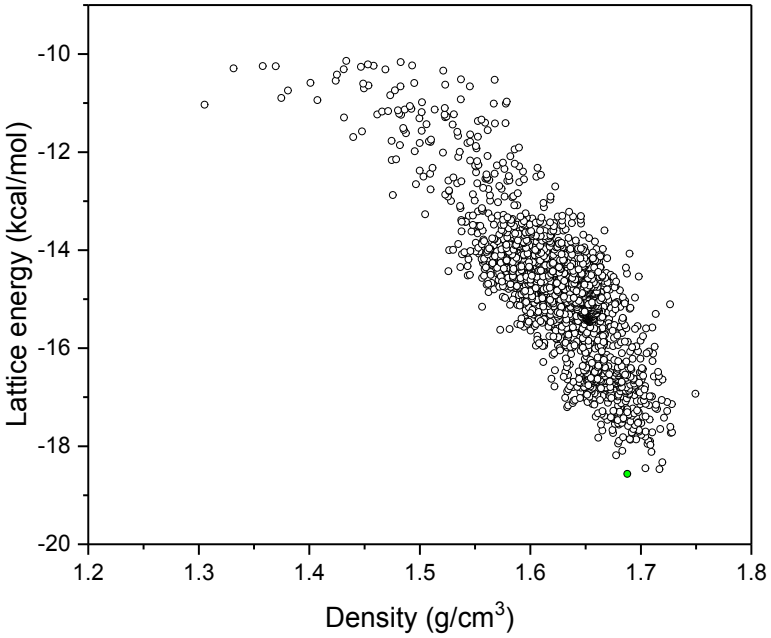

Figure S5. Scatter diagrams of lattice energy and density of co-crystal of ADN/ETN

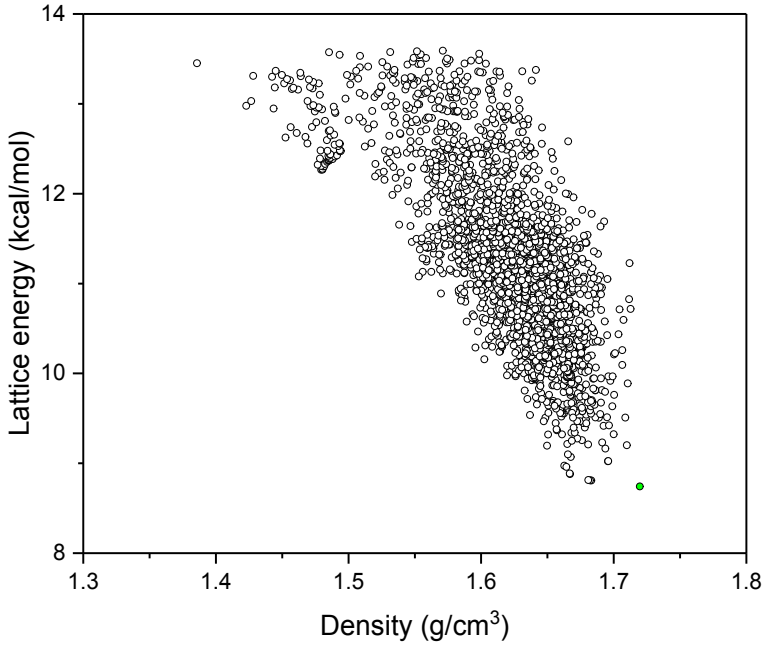

Figure S6. Scatter diagrams of lattice energy and density of co-crystal of ADN/RDX

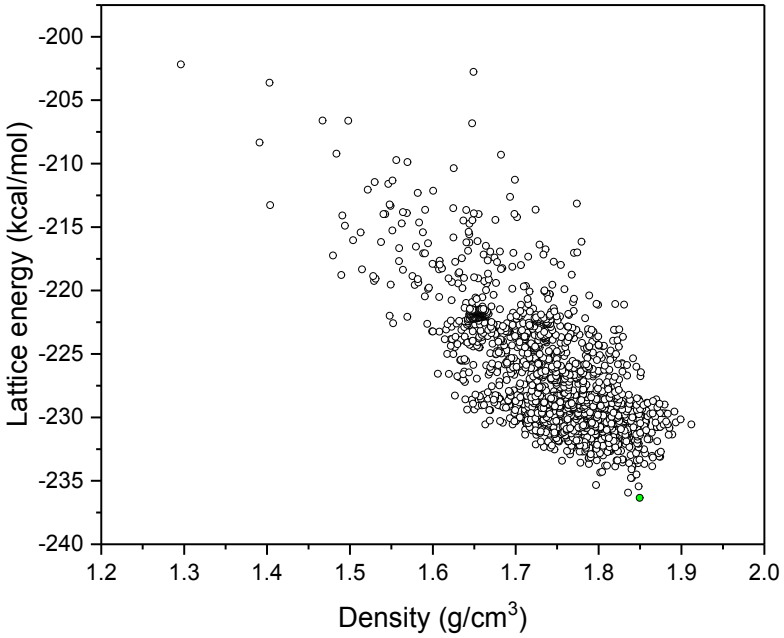

Figure S7. Scatter diagrams of lattice energy and density of co-crystal of ADN/TNB

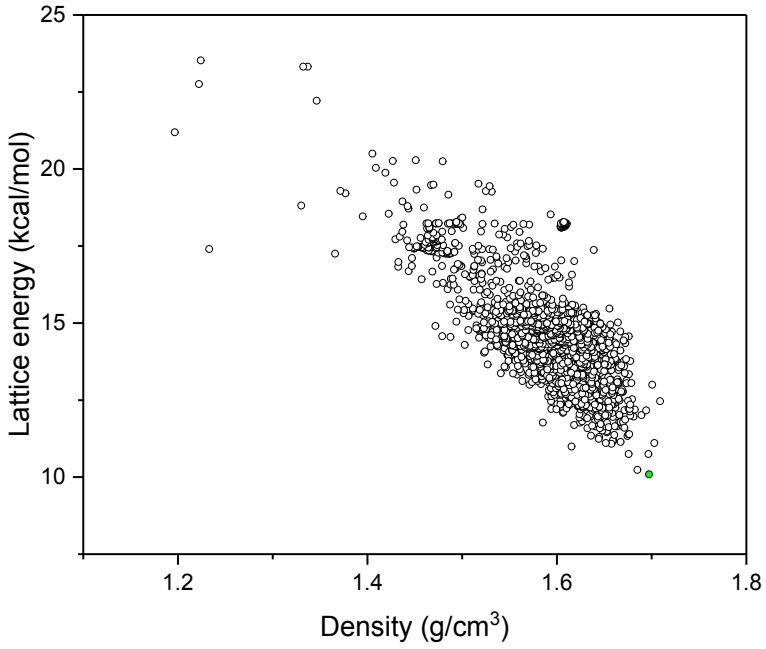

Figure S8. Scatter diagrams of lattice energy and density of co-crystal of ADN/MATNB

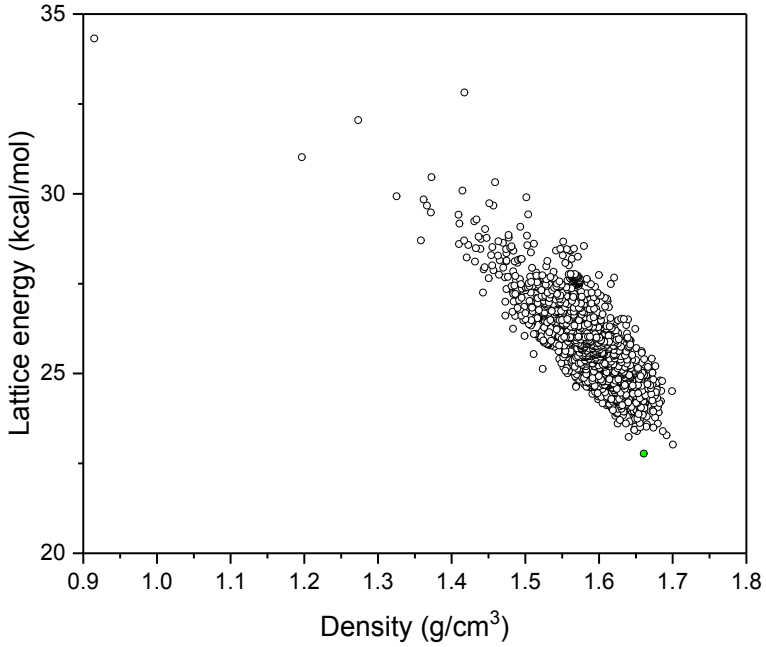

Figure S9. Scatter diagrams of lattice energy and density of co-crystal of ADN/TNAZ

2.2 Predictive packing diagrams of co-crystals

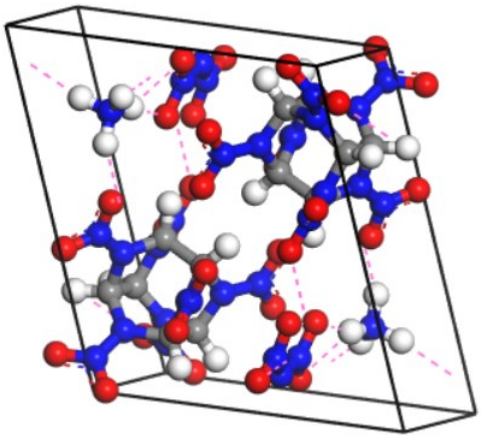

Figure S10. Predictive packing diagrams of ADN/CL-20 co-crystal

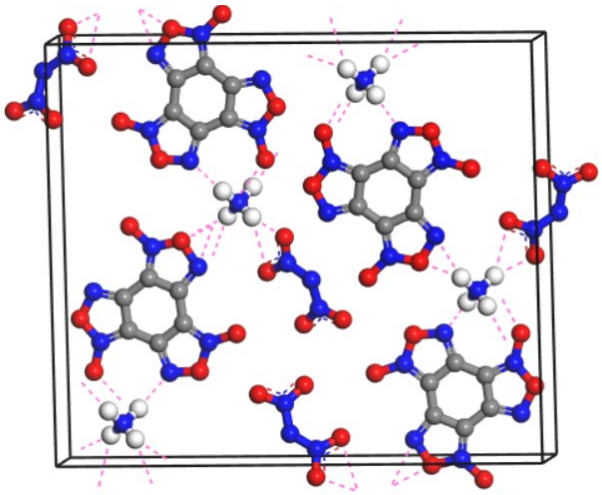

Figure S11. Predictive packing diagrams of ADN/BTF co-crystal

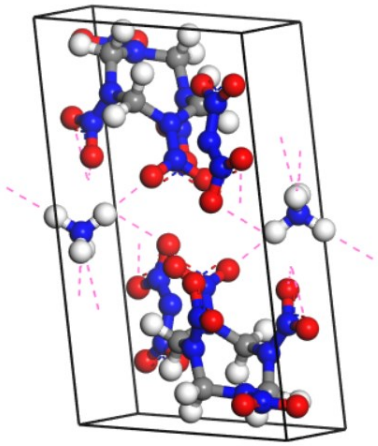

Figure S12. Predictive packing diagrams of ADN/HMX co-crystal

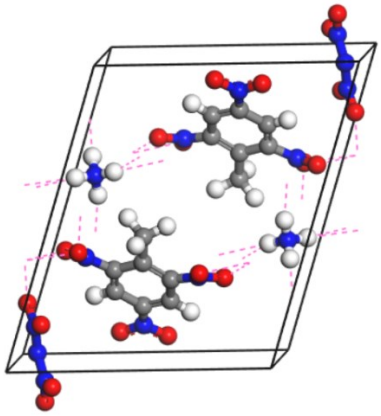

Figure S13. Predictive packing diagrams of ADN/TNT co-crystal

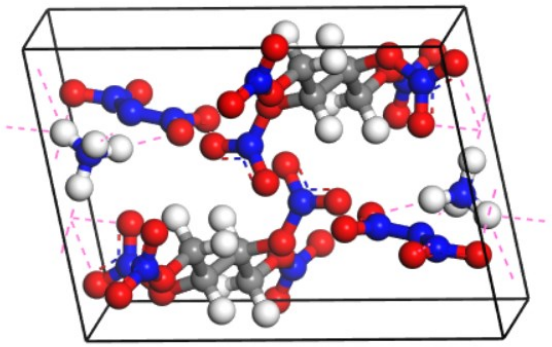

Figure S14. Predictive packing diagrams of ADN/ETN co-crystal

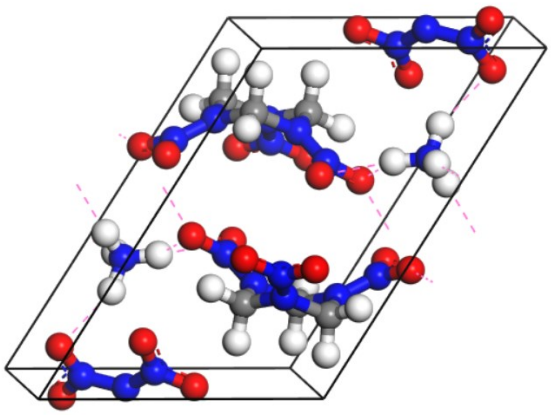

Figure S15. Predictive packing diagrams of ADN/RDX co-crystal

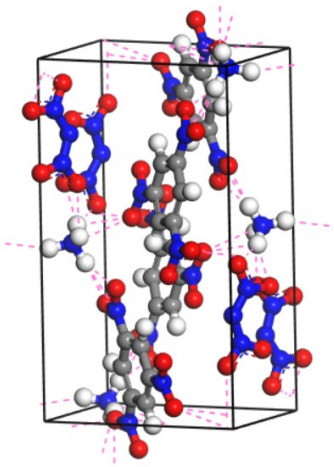

Figure S16. Predictive packing diagrams of ADN/TNB co-crystal

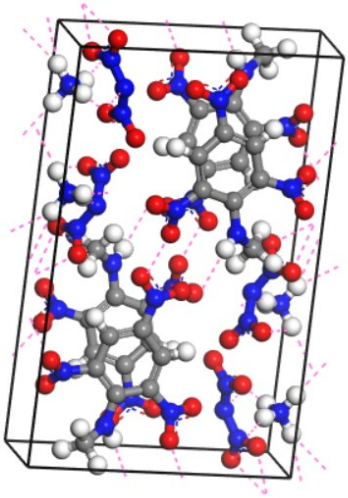

Figure S17. Predictive packing diagrams of ADN/MATNB co-crystal

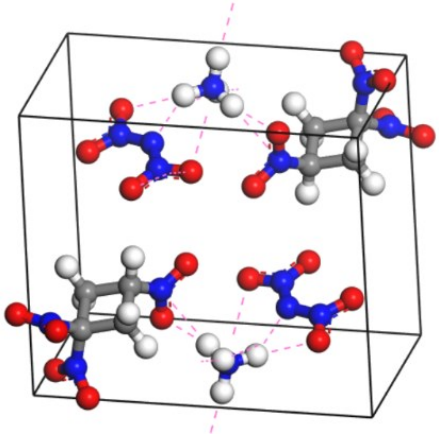

Figure S18. Predictive packing diagrams of ADN/TNAZ co-crystal

2.3 The lowest energy water sorption frames of co-crystal surfaces

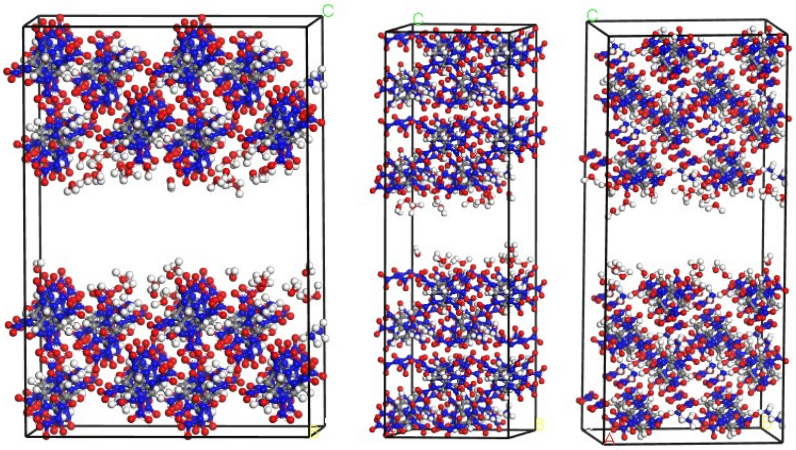

Figure S19. The lowest energy water sorption frames of (1 0 0), (0 1 0), (0 0 1) ADN/CL-20 co-crystal surfaces

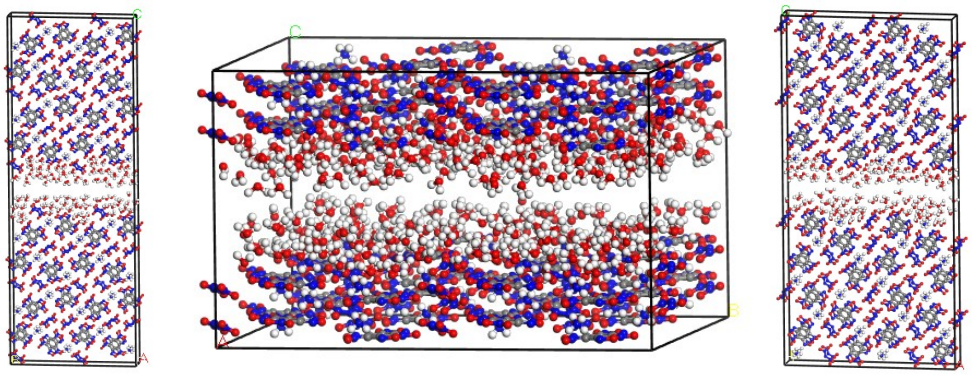

Figure S20. The lowest energy water sorption frames of (1 0 0), (0 1 0), (0 0 1) ADN/BTF co-crystal surfaces

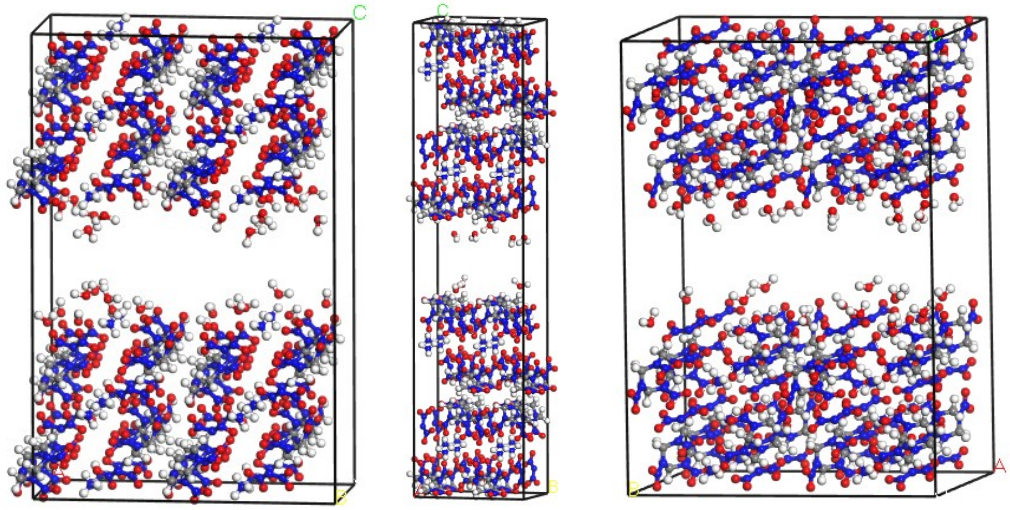

Figure S21. The lowest energy water sorption frames of (1 0 0), (0 1 0), (0 0 1) ADN/HMX co-

crystal surfaces

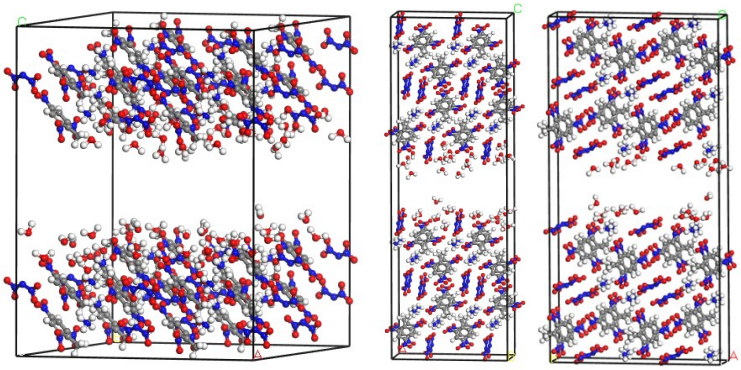

Figure S22. The lowest energy water sorption frames of (1 0 0), (0 1 0), (0 0 1) ADN/TNT co-crystal surfaces

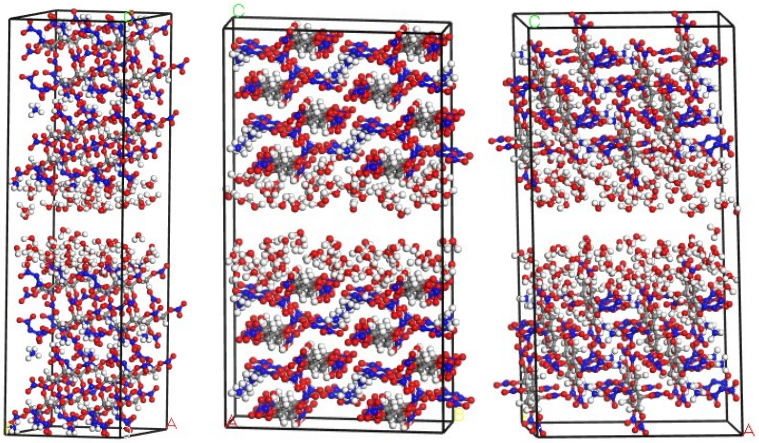

Figure S23. The lowest energy water sorption frames of (1 0 0), (0 1 0), (0 0 1) ADN/ETN co-crystal surfaces

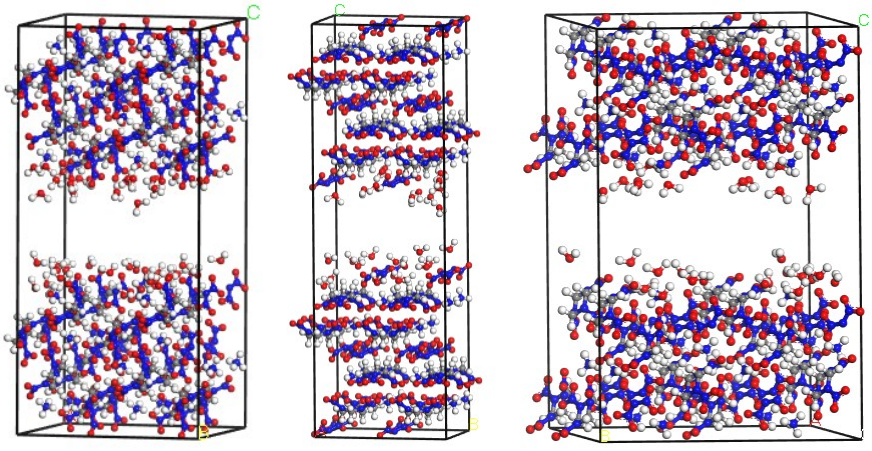

Figure S24. The lowest energy water sorption frames of (1 0 0), (0 1 0), (0 0 1) ADN/RDX co-crystal surfaces

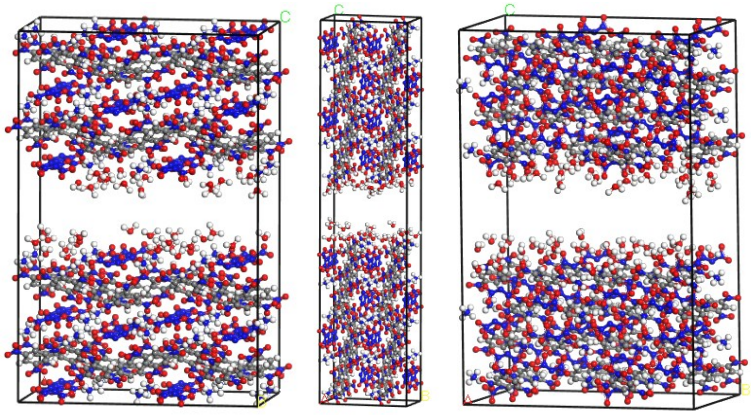

Figure S25. The lowest energy water sorption frames of (1 0 0), (0 1 0), (0 0 1) ADN/TNB co-crystal surfaces

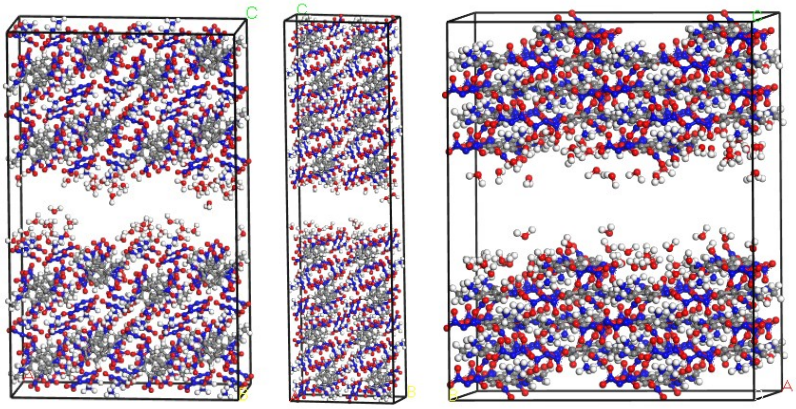

Figure S26. The lowest energy water sorption frames of (1 0 0), (0 1 0), (0 0 1) ADN/MATNB co-crystal surfaces

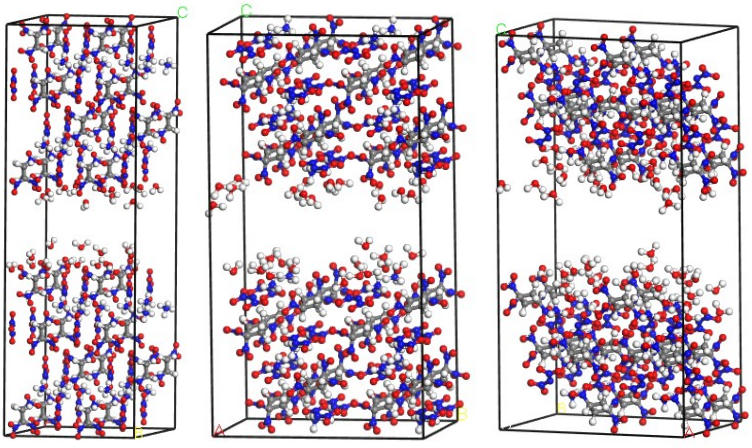

Figure S27. The lowest energy water sorption frames of (1 0 0), (0 1 0), (0 0 1) ADN/TNAZ co-crystal surfaces

3. Table captions

Table S1. ADN and selected guests' detonation properties[1-4]

Energetic Materials	Density (g/cm^3)	V_d (km/s)	P_d (GPa)	OB (%)	OBAC (%)	V_{gas} (cm^3/g)
ADN	1.81[1]	8.07[c1]	23.72[c1]	25.8[1]		987[1]
CL-20(ε)	2.04[1]	9.66[e1]	42.0[c2]	-11.0[1]	-2.85	827[1]
BTF	1.86[2]	8.5[e2]	36.0[e2]	-38.1[2]	-17.02	360[2]
HMX	1.91[1]	9.32[c1]	39.63[c1]	-21.6[1]	-7.62	886[1]
TNT	1.65[1]	6.88[e1]	19.53[e1]	-74.0[1]	-38.73	738[1]
ETN	1.70[3]	8.03[e3]	-	5.3[4]	11.26	704[3]
RDX	1.82[1]	8.98[c1]	35.17[c1]	-21.6[1]	-4.62	903[1]
TNB	1.69[2]	7.42[e4]	26.03[e4]	-56.3[4]	-26.10	600[4]
MATNB	1.68[4]	-	-	-72.68[4]	-39.32	-
TNAZ	1.84[1]	9.01[c1]	36.37[c1]	-16.7[1]	-12.69	877[1]

Notes: V_d：detonation velocity. P_d：detonation pressure, OB：oxygen balance. OBAC: oxygen balance after 1:1 cocrystallization. V_{gas}: gas formed by 1 g energetic materials at pressure of 1 bar. The c represents the computational values. The e represents experimental values.

Table S2. The computational details of oxygen balance after 1:1 cocrystallization

co-crystal materials	a	b	c	N	M_r	oxygen balance
ADN/CL-20	6	10	16	17	562.06	-2.85
ADN/BTF	6	4	10	11	376.06	-17.02
ADN/HMX	4	12	12	13	420.21	-7.62
ADN/TNT	7	9	10	8	351.19	-38.73
ADN/ETN	4	10	16	9	426.16	11.26
ADN/RDX	3	10	10	11	346.17	-4.62
ADN/TNB	6	7	10	8	337.16	-26.10
ADN/MATNB	7	10	10	9	366.20	-39.32
ADN/TNAZ	4	9	10	8	315.16	-12.69

Notes: a, b, c, N are the numbers of C, H, O, N atoms in one molecule, respectively. M_r represents the relative molecular mass.

Table S3. The computational details of water sorption capacity and sorption heat on ADN basic crystal faces and co-crystal faces

ADN and ADN-based co-crystals	vacuum slab (nm)	a (Å)	b (Å)	c (Å)	α (°)	β (°)	γ (°)	surface area (nm^2)	model density (g/cm^3)	model volume (Å)	adsorbed phase mass (g)	adsorbed phase volume (cm^3/g)	number of adsorbed water molecules	n_{ab} (mol/g)	n_{ex} (mol/g)	water sorption capacity (%)	wet air density (g/cm^3)	average adsorption heat（kcal/mol）	adsorption heat distribution （kcal/mol）
ADN 1 0 0	1	23.574	11.228	36.584	90	90	90	2.65	1.36	9683.28	$1.318*10^{-20}$	0.200	66	$8.315*10^{-3}$	$8.088*10^{-3}$	14.56	$1.13*10^{-3}$	21.846	3.412-35.712
ADN 0 1 0	1	11.228	13.828	54.734	90	90	100.4	1.55	1.07	12330.20	$1.318*10^{-20}$	0.105	31	$3.906*10^{-3}$	$3.787*10^{-3}$	6.82	$1.13*10^{-3}$	19.315	1.012-25.812
ADN 0 0 1	1	13.828	23.574	37.911	90	90	90	3.26	1.07	12358.30	$1.318*10^{-20}$	0.405	102	$1.285*10^{-2}$	$1.239*10^{-2}$	22.3	$1.13*10^{-3}$	20.771	1.912-36.912
CL-20ADN 1 0 0	1	29.37	20.45	42.31	90	90	93.12	6.01	1.18	25367.00	$2.986*10^{-20}$	0.347	37	$2.058*10^{-3}$	$1.666*10^{-3}$	3.00	$1.13*10^{-3}$	11.66	-0.088-16.632
CL-20ADN 0 1 0	1	20.45	17.05	55.97	90	90	95.55	3.49	1.54	19419.30	$2.986*10^{-20}$	0.132	16	$8.898*10^{-4}$	$7.406*10^{-4}$	1.33	$1.13*10^{-3}$	11.719	-1.288-16.712
CL-20ADN 0 0 1	1	29.37	20.45	42.31	90	90	93.12	6.01	1.38	21585.40	$2.986*10^{-20}$	0.203	25	$1.390*10^{-3}$	$1.161*10^{-3}$	2.09	$1.13*10^{-3}$	11.876	-0.888-18.212
BTF ADN 1 0 0	1	6.95	36.07	100.82	90	90	90	2.51	1.58	25278.00	$3.996*10^{-20}$	0.118	132	$5.485*10^{-3}$	$5.352*10^{-3}$	9.63	$1.13*10^{-3}$	40.461	3.912-79.112
BTF ADN 0 1 0	1	36.07	42.00	26.25	90	90	90	15.15	1.01	39756.20	$3.996*10^{-20}$	0.485	408	$1.695*10^{-2}$	$1.640*10^{-2}$	29.52	$1.13*10^{-3}$	20.442	1.312-36.912
BTF ADN 0 0 1	1	42.00	6.95	86.32	90	90	90	2.92	1.59	25205.60	$3.996*10^{-20}$	0.112	131	$5.444*10^{-3}$	$5.317*10^{-3}$	9.57	$1.13*10^{-3}$	35.02	4.412-62.212
HMX ADN 1 0 0	1	27.54	15.94	41.94	90	90	93.91	4.39	1.22	18369.90	$2.232*10^{-20}$	0.268	24	$1.786*10^{-3}$	$1.483*10^{-3}$	2.67	$1.13*10^{-3}$	11.01	0.112-15.712
HMX ADN 0 1 0	1	15.94	15.97	62.08	90	90	75.34	2.55	1.46	15294.20	$2.232*10^{-20}$	0.127	3	$2.232*10^{-4}$	$7.969*10^{-5}$	0.14	$1.13*10^{-3}$	8.53	0.012-11.612
HMX ADN 0 0 1	1	15.97	27.54	40.68	90	90	100.78	4.40	1.27	17576.90	$2.232*10^{-20}$	0.243	21	$1.562*10^{-3}$	$1.287*10^{-3}$	2.32	$1.13*10^{-3}$	10.99	-0.588-15.012
TNT ADN 1 0 0	1	27.24	22.71	37.29	90	90	72.61	6.19	0.85	22006.50	$1.866*10^{-20}$	0.624	63	$5.606*10^{-3}$	$4.901*10^{-3}$	8.82	$1.13*10^{-3}$	13.115	-0.288-20.512
TNT ADN 0 1 0	1	22.71	9.38	67.69	90	90	88.86	2.13	1.29	14410.30	$1.866*10^{-20}$	0.2	34	$3.026*10^{-3}$	$2.800*10^{-3}$	5.04	$1.13*10^{-3}$	14.846	-0.512-20.712
TNT ADN 0 0 1	1	9.38	27.24	53.56	90	90	83.19	2.56	1.37	13583.30	$1.866*10^{-20}$	0.147	18	$1.602*10^{-3}$	$1.436*10^{-3}$	2.58	$1.13*10^{-3}$	12.614	-0.512-19.412
ETN ADN 1 0 0	1	17.157	16.41	58.55	90	90	101.64	2.82	1.4	16141.80	$2.265*10^{-20}$	0.15	77	$5.645*10^{-3}$	$5.476*10^{-3}$	9.86	$1.13*10^{-3}$	20.88	1.312-33.512
ETN ADN 0 1 0	1	16.41	25.96	44.39	90	90	72.06	4.26	1.26	17987.50	$2.265*10^{-20}$	0.246	111	$8.138*10^{-3}$	$7.860*10^{-3}$	14.15	$1.13*10^{-3}$	18.40	1.512-33.012
ETN ADN 0 0 1	1	25.96	17.16	51.78	90	90	102.85	4.45	1.01	22488.50	$2.265*10^{-20}$	0.452	164	$1.202*10^{-2}$	$1.151*10^{-2}$	20.72	$1.13*10^{-3}$	17.93	1.512-34.812
RDX ADN 1 0 0	1	20.617	16.666	45.562	90	90	85.04	3.44	1.18	15597.10	$1.840*10^{-20}$	0.293	39	$3.520*10^{-3}$	$3.189*10^{-3}$	5.74	$1.13*10^{-3}$	12.991	0.412-18.712
RDX ADN 0 1 0	1	16.666	17.226	51.17	90	90	79.497	2.87	1.27	14444.40	$1.840*10^{-20}$	0.238	20	$1.805*10^{-3}$	$1.536*10^{-3}$	2.76	$1.13*10^{-3}$	11.563	-0.188-18.212
RDX ADN 0 0 1	1	17.226	24.04	38.188	90	90	73.79	4.14	1.21	15185.40	$1.840*10^{-20}$	0.264	22	$1.985*10^{-3}$	$1.687*10^{-3}$	3.04	$1.13*10^{-3}$	11.956	0.112-17.612

TNB ADN 1 0 0	1	30.45	17.49	46.96	90	90	90	5.33	1.43	25007.40	$3.584*10^{-20}$	0.162	35	$1.622*10^{-3}$	$1.439*10^{-3}$	2.59	$1.13*10^{-3}$	10.74	1.012-14.612
TNB ADN 0 1 0	1	17.49	18.94	76.33	90	90	73.84	3.31	1.48	24285.20	$3.584*10^{-20}$	0.144	47	$2.178*10^{-3}$	$2.015*10^{-3}$	3.63	$1.13*10^{-3}$	14.915	1.312-23.412
TNB ADN 0 0 1	1	18.94	30.45	47.31	90	90	90	5.77	1.31	27280.10	$3.584*10^{-20}$	0.233	65	$3.012*10^{-3}$	$2.749*10^{-3}$	4.95	$1.13*10^{-3}$	14.269	1.212-22.212
MATNB ADN 1 0 0	1	34.866	14.259	56.375	90	90	90	4.97	1.39	28026.38	$1.946*10^{-20}$	0.285	44	$3.755*10^{-3}$	$3.433*10^{-3}$	6.18	$1.13*10^{-3}$	12.861	0.112-17.912
MATNB ADN 0 1 0	1	14.259	23.487	81.241	90	90	90	3.35	1.46	26714.60	$1.946*10^{-20}$	0.195	25	$2.133*10^{-3}$	$1.913*10^{-3}$	3.44	$1.13*10^{-3}$	15.257	0.012-22.612
MATNB ADN 0 0 1	1	25.059	34.866	43.084	90	90	90	8.74	1.03	37643.60	$1.946*10^{-20}$	0.797	69	$5.888*10^{-3}$	$4.987*10^{-3}$	8.98	$1.13*10^{-3}$	12.164	-0.988-19.012
TNAZ ADN 1 0 0	1	17.31	13.76	54.68	90	90	72.92	2.38	1.35	12447.20	$1.675*10^{-20}$	0.155	22	$2.181*10^{-3}$	$2.006*10^{-3}$	3.61	$1.13*10^{-3}$	13.71	0.512-18.512
TNAZ ADN 0 1 0	1	13.76	22.68	43.13	90	90	95.51	3.12	1.25	13394.50	$1.675*10^{-20}$	0.224	27	$2.677*10^{-3}$	$2.424*10^{-3}$	4.36	$1.13*10^{-3}$	13.24	0.012-17.712
TNAZ ADN 0 0 1	1	22.68	18.68	44.41	90	90	97.29	4.24	0.92	18246.40	$1.675*10^{-20}$	0.531	49	$4.858*10^{-3}$	$4.258*10^{-3}$	7.66	$1.13*10^{-3}$	12.84	-0.788-20.712

Notes:

1. a, b, c, α, β, γ, vaccum slab, model volume, model density are model parameters, and the surface area was calculated as a × b. The mass was calculated according to the number of molecules in the model and avogadro's constant.

2. Wet air density was calculated by a simple empirical equation $\rho=0.0034843\left(P-0.3779\varphi P_S\right)/T$, where ρ is the density of air (g/cm³), ϕ is the relative humidity (%), P_s is the partial pressure of saturated vapor (Pa), T is the temperature(K), P is the total pressure of wet air(Pa). The equation was obtained from a Chinese reference published in Mining Safety & Environmental Protection, 2005, 32(4), 49-51. The authors constructed a math model and calculated wet air densities which were compared with the densities of real wet air.

Table S4. The computational details of the interaction between water molecule and crystal surface

Crystal	surface	Total energy (kcal/mol)	Water energy (kcal/mol)	Crystal surface energy (kcal/mol)	E_{int} (kcal/mol)	Average E_{int} (kcal/mol)
ADN	100	11401.69	4.46	11456.65	-59.41	-59.41
		11401.69	4.46	11456.65	-59.41	
		11401.69	4.46	11456.65	-59.41	
	010	14118.47	6.36	14182.07	-69.96	-70.25
		14118.47	6.36	14182.07	-69.96	
		14117.34	6.09	14182.07	-70.82	
	001	9887.15	3.02	9932.09	-47.96	-46.30
		9889.18	2.55	9932.09	-45.46	
		9889.18	2.55	9932.09	-45.46	
ADN/HMX	100	-1591.78	0.28	-1574.08	-17.98	-18.69
		-1592.20	0.37	-1574.08	-18.49	
		-1593.25	0.42	-1574.08	-19.59	
	010	-1210.70	0.59	-1192.46	-18.84	-19.10
		-1210.70	0.59	-1192.46	-18.83	
		-1211.46	0.63	-1192.46	-19.64	
	001	-1621.52	0.24	-1604.84	-16.92	-17.91
		-1624.88	0.36	-1604.84	-20.41	
		-1620.85	0.39	-1604.84	-16.41	
ADN/CL-20	100	-2351.67	0.19	-2339.16	-12.70	-16.31
		-2356.00	0.33	-2339.16	-17.17	
		-2357.91	0.30	-2339.16	-19.06	
	010	-2658.94	0.58	-2638.65	-20.87	-19.13
		-2656.68	0.40	-2638.65	-18.43	
		-2656.29	0.44	-2638.65	-18.08	
	001	-2457.69	0.42	-2438.54	-19.57	-18.89
		-2454.84	0.38	-2438.54	-16.69	
		-2458.64	0.32	-2438.54	-20.42	

Table S5. The parameters and value of the interaction site pairing energy difference of ADN/DPO based on virtual co-crystal screening method

Energetic Materials	$V_{s,max}$ (kcal/mol)	α	$V_{s,min}$ (kcal/mol)	β	E （kJ/mol）	Molar stoichiometry	E_{cc} （kJ/mol）	△E （kJ/mol）
DPO	41.13	2.14	-36.11	4.74	-10.12	1:1	-24.23	-0.93
						2:1	-48.45	-11.97

Notes: $V_{s,max}$:the maximum of molecular electrostatic potential. $V_{s,min}$: the minimum of molecular electrostatic potential. α:H-bond donor parameters. β: H-bond acceptor parameters. E_{cc}： the interaction site pairing energy of the co-crystal of stoichiometry 1n2m. △E: the value of the interaction site pairing energy difference.

4. Calculations related to ADN/18C6 co-crystal

According to the computational method above, the 18C6 crown ether is used to investigate the hygroscopicity of co-crystals. Because 18C6 crown ether belong to non-energetic materials with bad detonation performance and the application of ADN/18C6 co-crystal is hard, this section is put into the Supporting information. However, it is great and accessible to study on the hygroscopicity of co-crystal and verify our calculation method. The ADN/18C6 co-crystal has been experimental prepared successfully, which is from the Chinese reference: Preparation and Characterization of ADN/18C6 co-crystal, Chinese Journal of energetic materials, 2018, 26, 545-548.

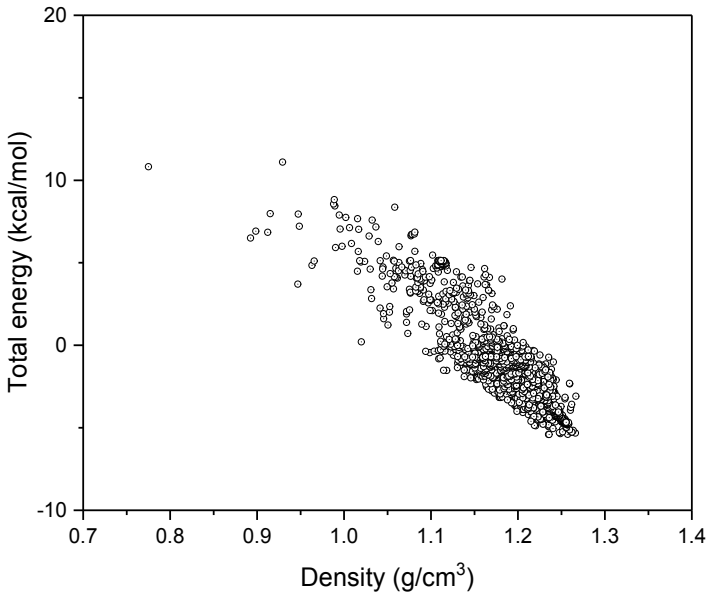

Figure S28. Scatter diagrams of lattice energy and density of co-crystal of ADN/18C6

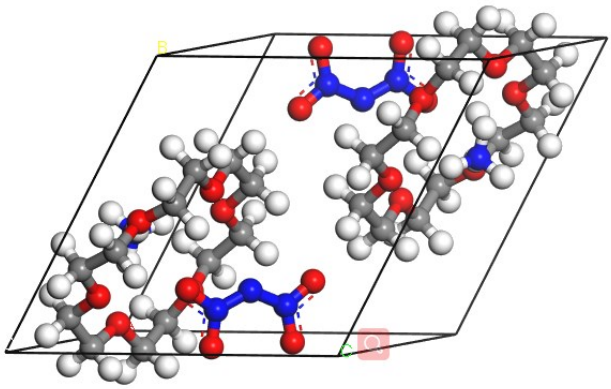

Figure S29. The predictive crystal structure of ADN/18C6

Table S6. The computational and experimental crystal parameters, density of ADN/18C6

Space group	V(Å^3)	A(Å)	B(Å)	C(Å)	α(°)	β(°)	γ(°)	ρ（g/cm^3）	Type
P-1	1019	11.03	10.88	10.82	66.21	60.99	87.87	1.27	Computational-Dreiding
C_2/C	3869.3	23.94	8.63	20.32	90	112.87	90	1.33	experimental

The predictive crystal structure is difference from the experimental crystal structure, and this difference could be caused by infeasible force field for 18C6 crown ether or caused by the hidden experimental structure. However, the predive density of 18C6/ADN co-crystal is 1.27g/cm^3 which is closed to the experimental density 1.33g/cm^3. Additionally, the experimental interaction is similar to predicted interaction. Next, as the Figure S7 shows, the computational water capacity has verified that 18C6 crown ether as co-crystal co-former can tun the hygroscopicity effectively. As the Table S7 and Equation 11, 14 shows the water sorption capacity can be tuned from 18.32% to 0.54% under 35℃, 50% relative humidity.From the view of experiments, the formation of ADN/18C6 make water sorption capacity rate of ADN reduce from 18% to 1.2% under 30℃, 80% relative humanity. The Y-axis data of Fig.5 is from Table S8 and Table S4. The X-axis data of Fig.5 is from BFDH crystal morphology prediction of co-crystal and water total sorption capacity calculations below. As the Table S9 shows, the △E of ADN/18C6 is -24.45 kcal/mol, which reveals that the co-crystal of ADN/18C6 can be prepared very likely, and it has been prepared experimentally.

Table S7. Water sorption capacity and adsorption heat ADN/18C6 co-crystal basic faces

ADN and ADN-based Co-crystals	Index of crystal face	Number of adsorbed water molecules	Water sorption capacity (%)	Average sorption heat（kcal/mol）	Sorption heat distribution（kcal/mol）
18C6	(1 0 0)	9	0.62	9.6	-0.29-13.41
	(0 1 0)	15	1.46	10.73	-0.19-14.81
	(0 0 1)	4	0	8.49	-0.29-10.71

Table S8. The computational details of the interaction between water molecule and ADN/18C6 co-crystal surface

Co-crystal	surface	Total energy (kcal/mol)	Water energy (kcal/mol)	Crystal surface energy (kcal/mol)	E_{int} (kcal/mol)	Average E_{int} (kcal/mol)
ADN/18C6	100	367.65	0.25	379.84	-12.41	-12.69
		369.12	0.22	379.84	-10.94	
		365.49	0.32	379.84	-14.68	
	010	571.55	0.36	587.94	-16.76	-14.69
		576.78	0.20	587.94	-11.36	
		572.22	0.23	587.94	-15.95	
	001	-104.12	0.31	-87.44	-16.99	-14.87
		-97.89	0.19	-87.44	-10.64	
		-104.12	0.31	-87.44	-16.99	

Table S9. The parameters and value of the interaction site pairing energy difference of ADN/18C6 based on virtual co-crystal screening method

Co-crystal co-former	$V_{s,max}$ (kcal/mol)	α	$V_{s,min}$ (kcal/mol)	β	E （kJ/mol）	Stoichiometry	E_{cc} （kJ/mol）	△E （kJ/mol）
18C6	14.18	0.63	-61.05	11.90	-7.47	1:1	-42.10	-21.45

Notes: $V_{s,max}$:the maximum of molecular electrostatic potential. $V_{s,min}$: the minimum of molecular electrostatic potential. α:H-bond donor parameters. β: H-bond acceptor parameters. E_{cc}： the interaction site pairing energy of the co-crystal of stoichiometry 1n2m. △E: the value of the interaction site pairing energy difference.

5. Predicted ADN/CL-20, ADN/HMX, ADN/18C6 co-crystal morphology by BFDH method and water total sorption capacity

After screening co-crystal co-formers, for evaluating the effect of reducing hygroscopicity accurately, a specify computational number is better than computational scope. Therefore, the problem related to water sorption capacity of co-crystal is simplified. First, BFDH method is used to predict crystal morphology. By the BFDH method, the co-crystal morphology can be predicted, the results of co-crystal is shown in the Table S10 and ADN crystal morphology prediction was listed in the reference 18.

Table S10. Results of ADN/CL-20, ADN/HMX, ADN/18C6 co-crystal morphology by the BFDH method.

Crystal	Indices of crystal face	Multiplicity	d_{hkl} (Å)	Distance (Å)	Total facet area (%)
ADN/CL-20	(0 1 0)	2	11.73	8.53	35.57
	(0 0 1)	2	10.08	9.93	27.36
	(1 -1 0)	2	8.48	11.79	25.13
	(0 1 -1)	2	8.23	12.15	6.58
	(1 -2 0)	2	6.96	14.36	1.07
	(1 -1 -1)	2	6.83	14.64	3.81
	(1 0 -1)	2	6.10	16.39	0.47
ADN/HMX	(0 1 0)	2	13.52	7.40	44.92
	(0 0 1)	2	7.71	12.97	21.55
	(1 0 0)	2	7.61	13.15	15.71
	(1 -1 0)	2	7.19	13.91	7.44
	(0 1 -1)	2	6.76	14.79	0.89
	(1 0 1)	2	6.23	16.04	6.00
	(1 -1 1)	2	6.04	16.54	3.50
ADN/18C6	(0 1 0)	1	19.52	5.12	11.69
	(0 -1 0)	1	19.52	10.25	11.69
	(1 0 0)	1	9.46	10.57	10.67
	(-1 0 0)	1	9.46	10.57	10.67
	(1 0 1)	1	9.04	11.07	9.03
	(-1 0 -1)	1	9.04	11.07	9.03
	(0 1 1)	1	8.54	11.71	7.295
	(0 -1 -1)	1	8.54	11.71	7.295
	(0 0 1)	1	8.49	11.77	5.63
	(0 0 -1)	1	8.49	11.77	5.63
	(1 1 1)	1	7.81	12.81	3.34
	(-1 -1 -1)	1	7.81	12.81	3.34
	(1 -1 0)	1	7.58	13.19	2.34
	(-1 1 0)	1	7.58	13.19	2.34

Table S11. The computational water sorption capacity of ADN/CL-20, ADN/HMX, ADN/18C6 co-crystal surface

Co-crystals	Indices of crystal face	Number of adsorbed water molecules	Water sorption capacity（%）	Average adsorption heat（kcal/mol）	Adsorption heat distribution（kcal/mol）
ADN/CL-20	(1 0 0)	37	3.00	11.66	-0.09-16.63
	(0 1 0)	16	1.33	11.72	0.29-16.71
	(0 0 1)	25	2.09	11.88	-0.89-18.21
	(1 -1 0)	62	5.47	12.91	0.012-19.01
	(0 1 -1)	41	3.42	11.80	0.91-17.61
	(1 -2 0)	47	3.78	11.54	-0.39-16.51
	(1 -1 -1)	50	4.05	11.89	0.41-17.91
	(1 0 -1)	37	2.70	10.9	-1.39-15.91
ADN/HMX	(1 0 0)	24	2.67	11.01	0.11-15.71
	(0 1 0)	3	0.14	8.53	0.01-11.61
	(0 0 1)	21	2.32	10.99	-0.58-15.01
	(1 -1 0)	33	3.72	12.47	0.91-18.11
	(0 1 -1)	34	3.87	12.50	0.81-17.31
	(1 0 1)	17	1.61	10.82	0.41-15.41
	(1 -1 1)	52	5.80	12.63	-0.09-21.41
ADN/18C6	(1 0 0)	10	0.76	9.53	-0.90-13.20
	(0 1 0)	16	1.59	10.64	-0.40-14.60
	(0 0 1)	5	0.06	8.43	-1.30-10.80
	(1 0 1)	5	0.14	8.49	-0.10-12.00
	(0 1 1)	8	0.51	7.57	-0.40-10.70
	(1 1 1)	18	1.18	9.23	-0.80-14.20
	(1 -1 0)	15	0.44	9.19	-0.70-13.20

Then, it is supposed that the hygroscopicity of crystal is originated from the hygroscopicity of different crystal surface. It can be express as Eq.11, where the θ_i, W_i refers to the percent of crystal surface area and the computational water sorption capacity of crystal surface, respectively.

$$W = \sum(\theta_i \bullet W_i) \quad (11)$$

The computational process of the water total sorption capacity of ADN, ADN/CL-20, ADN/HMX, ADN/18C6 co-crystal are expressed as respectively.

$$W_{ADN} = \sum(\theta_i \bullet W_i) = \frac{21.53\times14.56 + 20.10\times11.82 + 20.61\times21.26 + 29.50\times21.46 + 8.26\times25.33}{100} = 18.32\% \quad (12)$$

$$W_{ADN/CL-20} = \sum(\theta_i \bullet W_i) = \frac{35.57\times1.33 + 27.36\times2.09 + 25.13\times5.47 + 6.58\times3.42 + 1.07\times3.78 + 3.81\times4.05 + 0.47\times2.70}{100} = 2.85\% \quad (13)$$

$$W_{ADN/HMX} = \sum(\theta_i \bullet W_i) = \frac{44.92\times0.14 + 21.55\times2.32 + 15.71\times2.67 + 7.44\times3.72 + 0.89\times3.87 + 6.00\times1.61 + 3.50\times5.80}{100} = 1.59\% \quad (14)$$

$$W_{ADN/18C6} = \sum(\theta_i \bullet W_i) = \frac{11.69\times2\times1.46 + 10.67\times2\times0.62 + 9.03\times2\times0.01 + 7.295\times2\times0 + 5.63\times2\times0 + 3.34\times2\times0.92 + 2.34\times2\times0}{100} = 0.54\% \quad (15)$$

The Y-axis data of Figure 5 is from this section.

6. References

1 U. Teipel, Energetic Materials. Particle processing and characterization, WILEY-VCH, 2005.
2 Handbook of New Energetic Compound Data, Chemical Industry Press, 2016.
3 M. Kunzel, R. Matyas, O. Vodochodsky, J. Pachman, *Cent. Eur. J. Energ. Mater.*, 2017, **14**, 418-429.
4 Handbook of Energetic Materials and the Related Compounds, National Defense Industry Press, 2010.
5 M. M. Li, F. S. Li, R. Q. Shen, X. D. Guo, *J. Hazard. Mater.*, 2011, **186**, 2031-2036.
6 R. R. Sanghavi, P. J. Kamale, M. A. R. Shaikh, S. D. Shelar, K. S. Kumar, A. Singh, *J. Hazard. Mater.*, 2007, **143**, 532-534.
7 Y. Ma, L. Y. Meng, H. Z. Li, C. Y. Zhang, *CrystEngComm*, 2017, **19**, 3145-3155.
8 X. F. Wei, Y. Ma, X. P. Long, C. Y. Zhang, *CrystEngComm*, 2015, **17**, 7150-7159.
9 Y. Ma, A. B. Zhang, X. G. Xue, D. J. Jiang, Y. Q. Zhu, C. Y. Zhang, *Cryst. Growth Des.*, 2014, **14**, 6101-6114.
10 P. Politzer, J. S. Murray, *Cryst. Growth Des.*, 2015, **15**, 3767-3774.
11 A. R. Oganov, C. J. Pickard, Q. Zhu, R. J. Needs, *Nat. Rev. Mater.*, 2019, **4**, 331–348.
12 S. L. Mayo, B. D. Olafson, W. A. Goddard, *J. Phys. Chem.*, 1990, **94**, 8897−8909.
13 Y. H. Lan, J. X. Zhai, D. H. Li, R. J. Yang, *J. Mater. Sci.*, 2015, **50**, 4933-4939.
14 M. Vasileiadis, C. C. Pantelides, C. S. Adjiman, *Chem. Eng. Sci.*, 2015, **121**, 60–76.
15 M. Zhang, Z. Z. Liang, F. Wu, J. F. Chen, C. Y. Xue, H. Zhao, *J. Cryst. Growth*, 2017, **467**, 47–53.
16 G. R. Desiraju, *Angew. Chem. Int. Ed.*, 2007, **46**, 8342–8356.
17 R. M. Bhardwaj,; J. A. McMahon, J. Nyman, L. S. Price, S. Konar, I. D. H. Oswald, C. R. Pulham, S. L. Price, *J. Am. Chem. Soc.*, 2019, **141**, 13887−13897.
18 X. J. Chen, L. C. He, X. R. Li, Z. Y. Zhou, Z. Q. Ren, *J. Phys. Chem. C*, 2019, **123**, 10940-10948.
19 O. Talu, A. L. Myers, *AIChE J.*, 2001, **47**, 1160-1168.
20 M. Ito, K. Nambu, A. Sakon, H. Uekusa, E. Yonemochi, S. Noguchi, K. Terada, *J. Pharm. Sci*., 2017, **106**, 859-865.
21 M. Murase, R. Ohta, *J. Phys. Chem. C*, 2019, **123**, 13246–13252.
22 D. Musumeci, C.A. Hunter, R. Prohens, S. Scuderi, J.F. McCabe, *Chem. Sci.*, 2011, **2**, 883-890.
23 T. Grecu, C.A. Hunter, E.J. Gardiner, J.F. McCabe, *Cryst. Growth Des.*, 2014, **14**, 165-171.
24 M. K. Corpinot, D. K. Bucar, *Cryst. Growth Des.*, 2019, **19**, 1426−1453.
25 M. C. Etter, *J. Phys. Chem.*, 1991, **95**, 4601−4610.